Leadership in Sustainable Infrastructure
Leadership en Infrastructures Durables

Vancouver, Canada
May 31 – June 3, 2017/ *Mai 31 – Juin 3, 2017*

UNDERSTANDING THE RESPONSE OF REINFORCED CONCRETE SLABS DUE TO CONTACT EXPLOSION OF TNT

Dua, Alok[1,4], Braimah, Abass[2], Matsagar, Vasant[3]
[1,2] Carleton University, Canada
[3] Indian Institute of Technology (IIT) Delhi, India
[4] alok.dua@carleton.ca

Abstract: Evaluating response of reinforced concrete (RC) structures to blast loads is now a matured field of research. The United Facilities Criteria (UFC) 3-340 design manual and similar other manuals lay out the design practice for blast resistant structures. However, most of the design methodologies are restricted to far-field (scaled distance > 1.18 m/kg$^{1/3}$) blast loading. The semi-empirical charts and equations presented in design manuals for far-field blast loading are not accurate in the near-field events and furthermore very little research is available on contact explosions. Contact explosions are more complex than the far-field explosion effects due to the spatially and temporally non-uniform overpressure. There are limited experimental studies available in the literature as many gauges do not survive the harsh near-field environment. Thus, most finite element models in the near-field events are validated based on post blast damage photos. This paper presents the results from field tests conducted on RC slabs with embedded piezo-electric based concrete vibration sensors (CVS). A correlation has been shown between the concrete strains and the voltage recorded by the sensors. These results have further been compared to the numerical results obtained from LS-DYNA. The contact explosion was modeled using the arbitrary-Lagrangian-Eulerian (ALE) element formulation. The study shows that contact explosion can be reliably modeled using the presented parameters. The readings obtained from CVS could capture the shock wave propagation and the strain time history in the slab at required locations.

1 Introduction

Design of structures to resist blast loads is performed with guidelines laid out in design manuals from various government agencies like Federal Emergency Management Agency and United Facilities Criteria (FEMA 426, 2005; UFC-3-340-01, 2002; UFC-3-340-02, 2008; UFC-4-010-01, 2007; UFC-4-010-02, 2007). Broadly, the design approach recommends maintaining a minimum standoff distance while designing the structural members to resist the blast loads from far-field range. Most of these manuals have been specifically developed for defense purpose, however they have now been adopted for use in civilian structures. The far-field scenario may not be applicable to every situation and certainly not applicable at places with high population density where it is not possible to maintain a minimum standoff distance. A close look at terrorist attacks in the last few decades reveals that most of the attacks were in close range of the target, be it a vehicle-borne or person-borne device (Ducibella & Cunningham, 2010).

The current design procedure involves generation of blast load parameters from the charts or empirical relationships based on scaled distance. These blast parameters are qualitatively accurate in far-field range but lose accuracy in near-field range. In near-field range, the blast pressures are highly non-uniform spatially as well as temporally (Figure 1). Additionally, there are probably no gauge that can satisfactorily measure the blast pressures close to the point of detonation. These factors are more pronounced for contact explosion scenario wherein the temperature in the fireball is extremely high. Moreover, a contact

explosion results in local response and damage to structural elements while the global response is negligible. There is limited research available in the literature on contact explosion response of structural members. Most of the work done in the past is based on numerical simulations and are not validated with field data (Dua & Braimah, 2016). This paper presents data acquired from field experiments conducted by subjecting reinforced concrete (RC) slabs to contact explosion of 500 grams of tri-nitro-toluene (TNT) explosive. The slabs were embedded with concrete vibration sensors (CVS) on top and bottom, to measure the stain response time history at pre-determined locations. The results are compared with the numerical simulations with an aim to calibrate the model parameters. The outcome of the study will be used for further research on contact explosion response of RC columns.

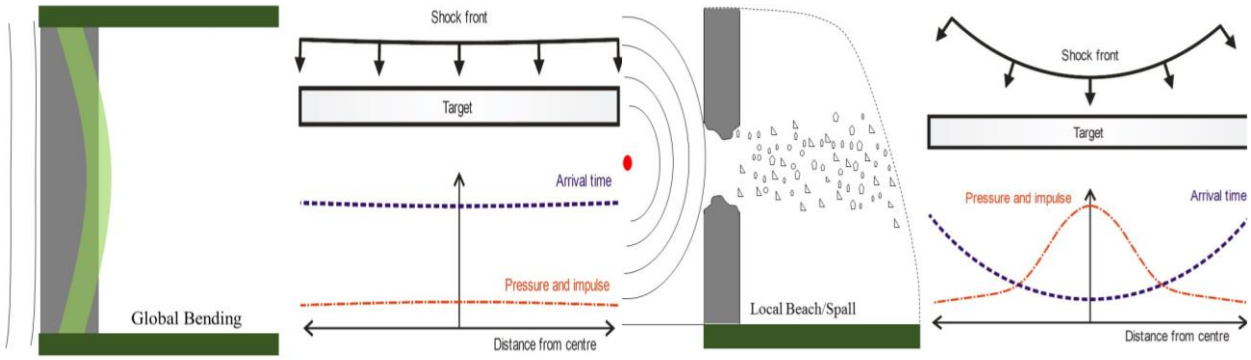

Figure 1: (a) Far-field explosion (global response) (b) Near-filed explosion (local response) (Rigby et al., 2014)

2 Experimental Program

2.1 Preliminary Trials

Preliminary trials were conducted to design the thickness and dimensions of the slab to be used for ascertaining the proper functioning of CVS. Plain concrete slab of 750 × 750 × 75 mm were subjected to 500 grams TNT explosion, (Figure 2-(a)). Complete slab perforation was observed due to the contact explosion. Based on this observation, reinforced concrete (RC) slab of 750 × 750 × 100 mm was subjected to same explosive weight, which also resulted in perforation. Additionally, the scab on the bottom face was very close to the edges, (Figure 2-(b)).

Figure 2: Preliminary tests for contact explosion on (a) PC slab (b) RC slab

The inputs assisted in finalizing the final slab dimensions of 900 × 900 × 200 mm for examining efficacy of the CVS. Two regular reinforcement bar (rebar) mats of 12-mm diameter at 100 mm c/c were provided at top and bottom with 30 mm cover and the CVS were placed 200 mm apart (Figure 3).

2.2 Experimental Setup

Two concrete panels of 35 MPa strength embedded with five CVSs were cast for the experimental tests. Adequate marking scheme was devised for the output cables of the CVS before pouring the concrete. The concrete was poured till the level reached the CVS top. Technical details of the CVS can be obtained from Bhalla et al. (2011); Bhalla and Kaur (2014); Talakokula and Bhalla (2014). The range of voltage expected to be developed across the CVS was predetermined using Equation 1. It is assumed that the strain in concrete is compatible with the strain developed in the piezoelectric (PZT) material embedded inside the CVS. The parameters used in Equation 1 are presented in Table 1.

[1] $$V = \frac{d_{31}\overline{Y^E}h(S_1+S_2)}{\overline{\varepsilon_{33}^T}(1-\nu)}$$

Table 1: Properties of PZT patch used in CVS (Bhalla & Kaur, 2014)

PZT size mm^2	Thickness (h) mm	Piezoelectric strain coefficient (d_{31}) m/V	Young's Modulus (Y^E) N/m^2	Poisson's ratio (ν)	Electric permittivity (ε_{33}^T) Farad/m
10×10	0.2	-2.1×10^{10}	6.667×10^{10}	0.3	2.124×10^{-8}

The peak strain (S_1 + S_2) in the two principal axial directions were estimated from preliminary numerical simulation for the setup. The estimated peak voltage derived via Equation 1 was required to set the oscilloscope resolution in order to correctly capture the event. Two Tektronix 3054C models were used for capturing the voltages developed in the CVS. The triggered event was captured for 10 ms in the first test and later corrected to 4 ms for the second test. The trigger voltage was set to 0.1 V. The complete test setup before the detonation and during the detonation is presented in Figure 3-(c) and Figure 3-(d) respectively.

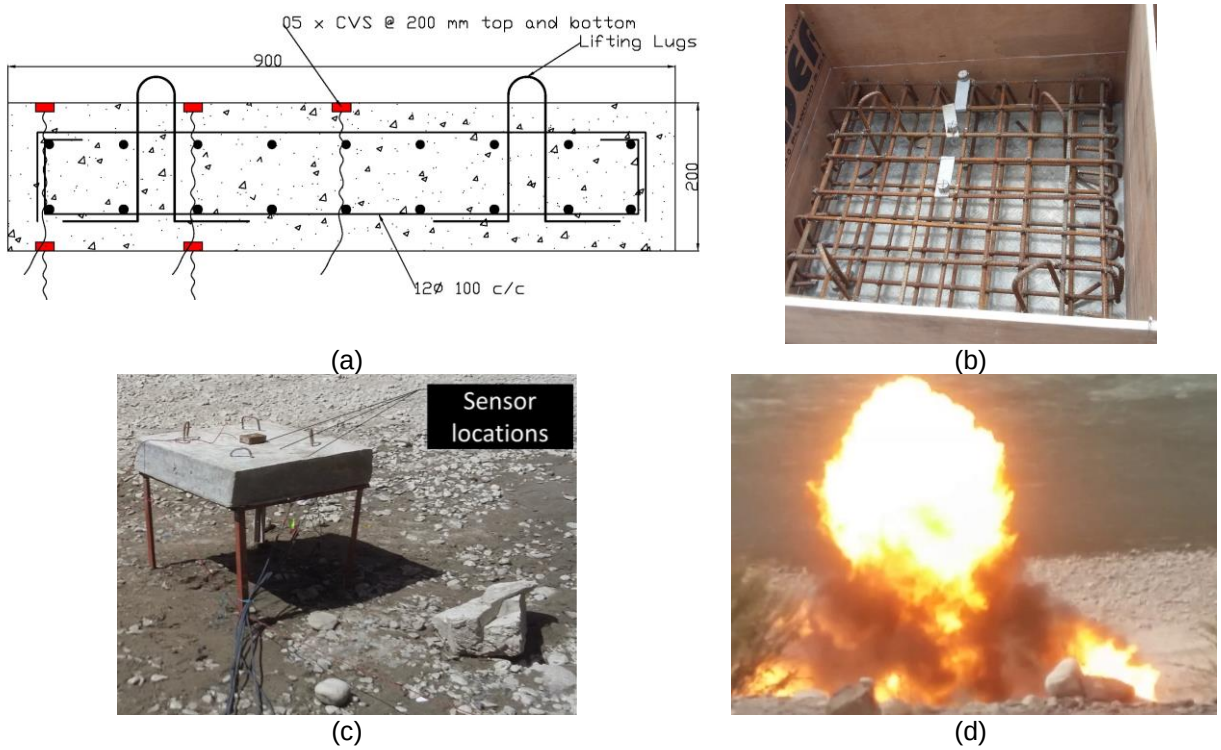

(a) (b)

(c) (d)

Figure 3: (a) Slab cross-section (b) Rebars and CVS before concreting (c) Experimental setup (d) Fireball during data acquisition

2.3 Experimental Results

The two slabs were subjected to a contact explosion of 500 grams of TNT block with 120 × 80 × 40 mm dimensions. The TNT block was placed at the centre with the 120-mm side perpendicular to the line of embedded CVSs. The CVS embedded at the point of detonation did not survive the event in both the tests and no readings were obtained. The contact explosion did not cause perforation in the slab and only top face cratering and bottom scabbing were observed. The top layer rebars were deflected (bent) while the bottom layer rebars suffered no bending. In the second test the bottom CVS at 200 mm from the point of detonation was damaged; however initial readings were recorded by the oscilloscope. The recorded data is tabulated in Table 2 and two post-event photos showing the top face catering are presented in Figure 4.

Table 2: Experimental results

Test No.	Crater diameter (mm)		Scab diameter (mm)		Crater depth (mm)
	Shorter side	Longer side	Shorter side	Longer side	
1	400	380	500	525	95
2	420	400	500	520	100

(a) (b)

Figure 4: (a) Crater on detonated face (b) Scab diameter at bottom face

The data acquired from the oscilloscopes is presented in Figure 5.

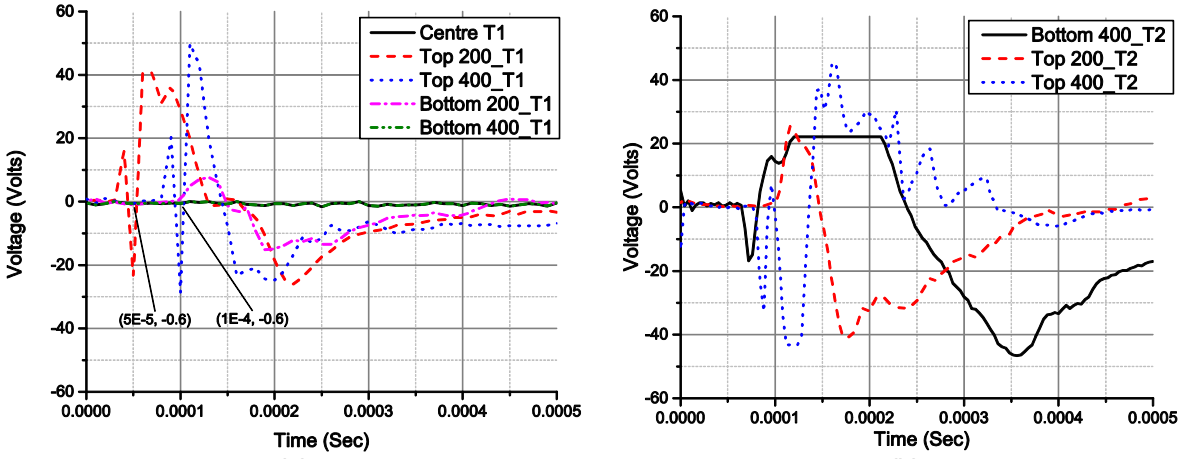

(a) (b)

Figure 5: Voltage time histories (a) Test 1 (b) Test 2

It can be observed from Figure 5-(a) that the shock wave arrived at the top sensors first and later at the bottom sensors. The arrival time of the shock wave at top sensor at 200 mm was 0.03 ms and that of top sensor at 400 mm was 0.08 ms thereby estimating the wave velocity as 4000 m/s. The readings from second test have better resolution as the event was recorded for 4 ms, however for future tests a duration

of data acquisition of 2-2.5 ms would be required. The voltage resolution for a 500 gram TNT explosion was observed to be greater than 50 V. The readings from bottom sensors at 400 mm from the point of detonation were not found to be appropriate. This may be due to the fact that the sensors were atop the steel frame on which the slab was placed. Further tests will avoid this situation by embedding the sensors away from the edges. The converted time history of effective strains in principal directions has been discussed with the numerical results.

3 Numerical Simulations

3.1 Preliminary Investigations

LS-DYNA incorporates modeling of detonation process via the arbitrary-Lagrangian-Eulerian (ALE) elements (Puryear, 2012; Trajkovski et al., 2014) or by using *LOAD_BLAST keyword (Goel et al., 2015). The pressure loading developed due to detonation of an explosive can be coupled with a Lagrangian part to model the fluid structure interaction (FSI). This is done with the *CONSTRAINED_LAGRANGE_IN_SOLID (CLIS) keyword using penalty type coupling (CTYPE 5). Preliminary investigations were carried out for the blast pressures developed by the detonation process in LS-DYNA. The keyword parameters and mesh sensitivity were examined both in 2D and 3D modeling (Figure 6).

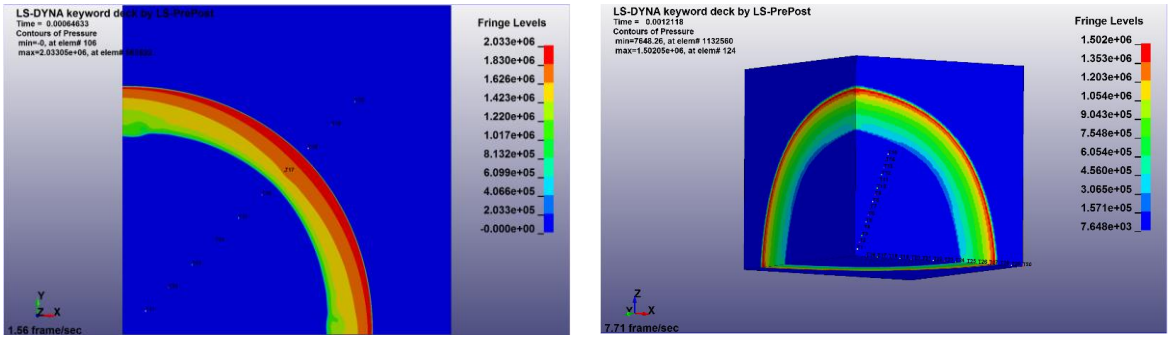

(a) (b)

Figure 6: Blast pressure levels due to detonation of 27 kg TNT (a) 2D formulation (b) 3D formulation

The peak overpressure due to detonation of 27-kg TNT charge at a scaled distance of 0.667 kg/m$^{1/3}$ were compared with ConWep (Hyde, 1988) results for varied element sizes. It was observed that the peak overpressures are mesh dependent and a mesh sensitivity study must be carried out before further studies. An element size of 20 mm was found to be computationally efficient for a 3D formulation and resulted in minimal error of peak overpressure and impulse when compared to ConWep results (Figure 7).

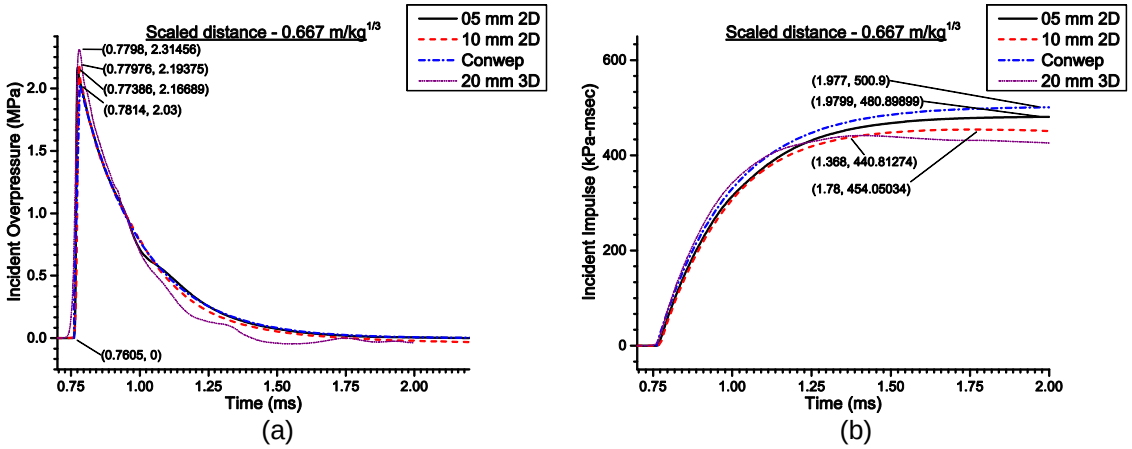

(a) (b)

Figure 7: Mesh sensitivity (a) Peak overpressure (b) Impulse

For the purpose of this study an element size of 10 mm was used. It is recommended that equal sized elements be used for air as a simulation with biased mesh was tried which resulted in longer computational time.

The parameters in *CONTROL_ALE keyword are important in order to get accurate peak overpressures and duration. LS-DYNA keyword manual recommends alternate advection logic (EQ.-1) for explosive simulations which can be invoked by the DCT flag in *CONTROL_ALE keyword. It also recommends Van leer + Half-index-shift (EQ.-2) as the advection method for the METH flag. Any other option for these variables resulted in improper decay i.e. shorter time duration in the pressure-time history which is not an actual representation of a blast event.

Table 3: Parameters for *CONTROL_ALE keyword

Variable	DCT	NADV	METH	AFAC	EBC	PREF
Value	-1	1	-2	-1	2	101 kPa

3.2 Geometric and Constitutive Modeling

A quarter symmetric model was prepared to achieve computational efficiency. The TNT block and air around it were modeled as ALE elements and the nodes at the boundary were merged. An average element size of 10 mm was used for the TNT block and air, however it was biased towards the point of detonation. The air was modeled beyond the slab to allow the blast pressure to vent out and not get reflected from the boundary. Although LS-DYNA provides *BOUNDARY_NON_REFLECTING keyword, this seems to work only for Lagrangian elements and not applicable to ALE elements as observed from the initial models prepared for this study. Concrete slab and rebar were modeled as Lagrangian elements. An element size of 5 mm was used for the whole slab. *CONTRAINED_LAGRANGE_IN_SOLID keyword was used to couple the rebars with the concrete and constrain the rebar with an acceleration and velocity as in concrete elements (CTYPE 2). The final model is presented in Figure 8.

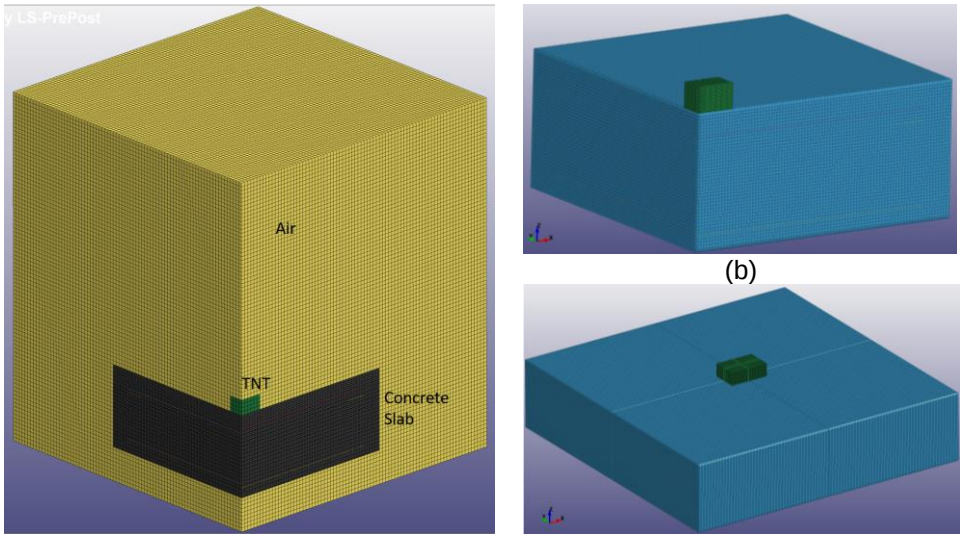

Figure 8: LS-DYNA model (a) Quarter model showing all parts (b) Quarter model showing TNT and concrete slab (c) Full model showing TNT and concrete slab

The concrete slab was modeled with *MAT_CSCM (Mat_159), continuous surface cap model (CSCM) constitutive law which is based on another study on full metal jacket projectile impact on plain concrete panels. It was concluded from this study that CSCM material law for concrete can efficiently predict the cratering and scabbing behavior compared to other models. Albeit it is a known fact that concrete shows strain-rate dependent behavior, it is inappropriate to account for the same in finite element modeling. It has

been reported in the literature that even models that do not employ rate-effects are still able to show strain-rate dependency. Concrete exhibits strength increase at high strain-rate due to inertial effects which is inherently included in material law hence an additional increase is not required (Schwer, 2009; Williams & Williamson, 2011). It was also observed from the projectile impact studies, that concrete panels behaved unrealistically stiff with strain-rate effects activated and no crater or scab was formed on the impact face and back face respectively as observed from the experimental results (Figure 9). The rebars were modeled with *MAT_PIECEWISE_LINEAR_PLASTICITY (Mat_024). Other parameters used for the model were as reviewed in a previous paper (Dua & Braimah, 2016).

(a) (b) (c)

Figure 9: FMJ projectile impact (a) Impact face crater (b) Back face scab (c) Panel cross-section showing crater and scab

3.3 Numerical Results and Discussion

Numerical simulation with the parameters presented above was run for 0.45 ms on an Intel Xeon 2.8 GHz processor with 18 GB RAM which took three hours to complete. The TSSFAC parameter in *CONTROL_TIMESTEP keyword is recommended to be set at 0.2 or lesser to avoid error termination. Top and bottom views of the slab depicting the contact face crater and bottom scab are presented in Figure 10.

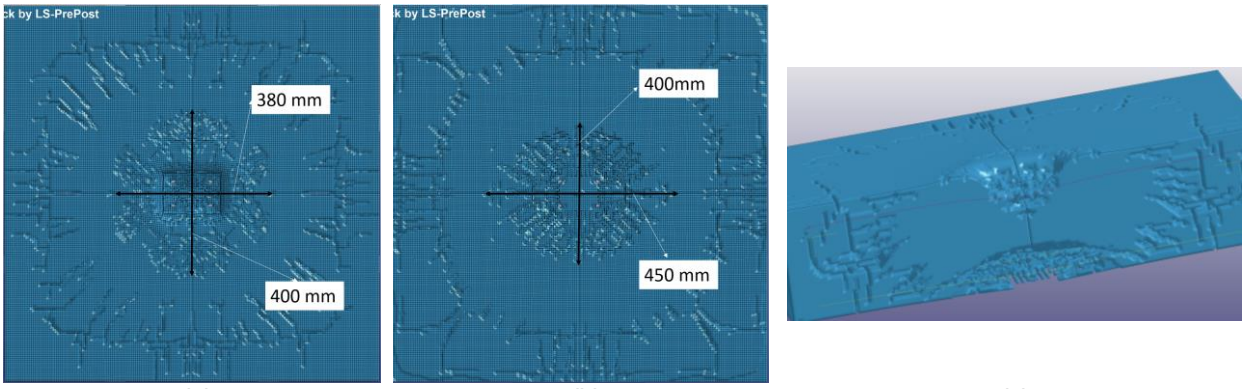

(a) (b) (c)

Figure 10: Numerical results (a) Contact face crater (b) Bottom face scab (c) Slab cross-section

It was observed that the crater size on the contact face was predicted close to the experimental observations. Scabbing was produced on the bottom face due to reflection of shock waves causing tensile failure. The dimensions of the scab were found to be lesser than the experimental observations. The recorded data is tabulated in Table 4.

Table 4: Comparison of numerical and experimental observations

Parameter observed	Contact face Crater		Back Face Scabbing		Crater Depth
	Shorter Side mm	Longer Side mm	Shorter Side mm	Longer Side mm	mm
Experimental	410	390	500	520	95
Numerical	400	380	425	450	75
Error %	2.5	2.5	15	13.5	20

The stress-strain curve for two elements that were eroded in compression and tensile failure respectively, is presented in Figure 11. It can be observed that the element failed at a stress value higher than the specified concrete compressive strength of 35 MPa and tensile strength of 4.1 MPa in the model. This is consistent with the previous statement that an additional increase of the strength to cater for strain-rate effect is inappropriate. However, it is to be noted that this strength increase was observed only with TSSFAC values of <0.2. At larger time-step values the strength increase was not observed and the elements failed at 35 MPa compressive strength.

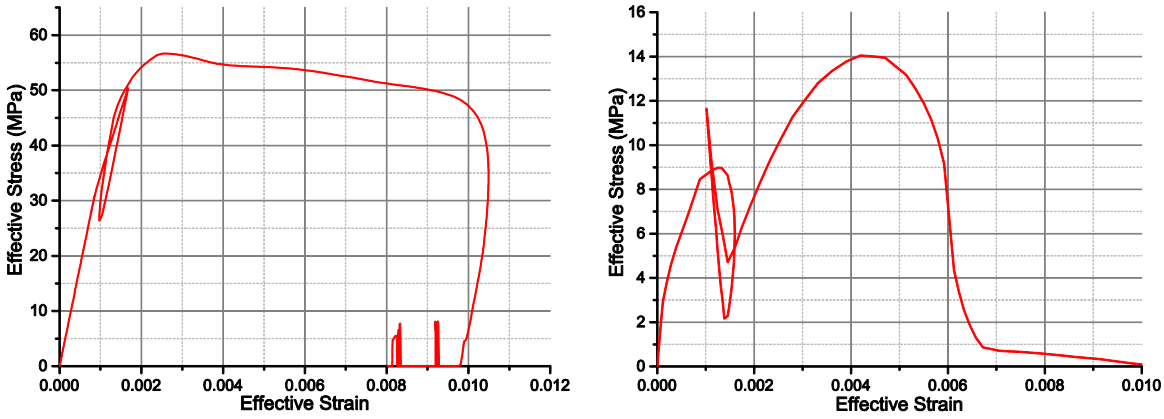

(a) (b)

Figure 11: Stress-Strain curves (a) Compressive failure (b) Tensile failure

The effective strain from the LS-DYNA simulation was plotted with the strain recoded by the CVS and is presented in Figure 12.

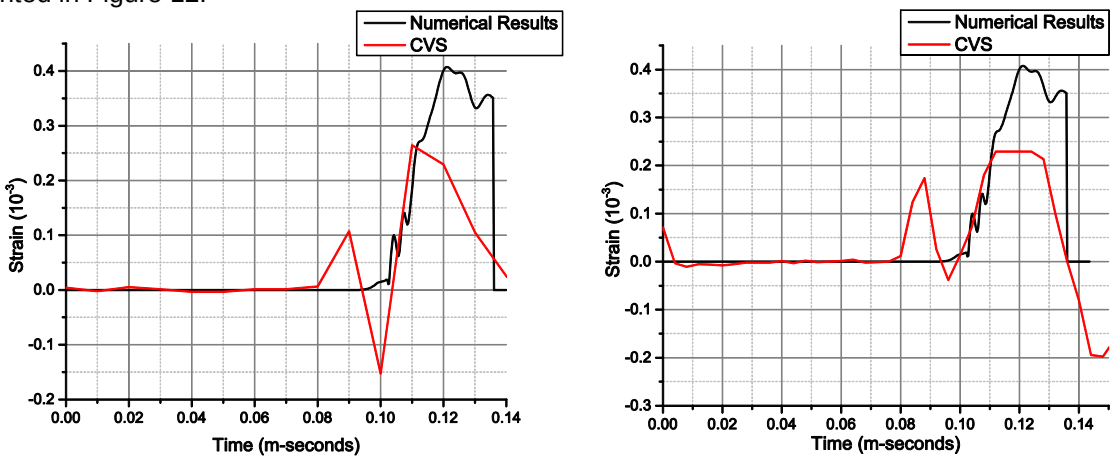

(a) (b)

Figure 12: Numerical results vs output of CVS on top at 400 mm (a) Test 1 (b) Test 2

It can be seen that the arrival time of the shock wave is correctly captured by the CVS. However, the strain values show a discrepancy between the two results. This can be attributed to the fact that Equation 1 is applicable in elastic range only and may not be applicable for high strain-rate problems. The CVS is required to be calibrated for the anticipated strain rates from a contact explosion. The voltage resolution and acquire duration is recommended to be 40 V and 0.25 ms respectively for future tests involving 500 grams TNT explosive.

4 Conclusions

In this study, RC slabs were subjected to 500 grams of TNT explosion in contact. The slabs were embedded with concrete vibration sensors (CVS) to record the time history of strain in the concrete at five locations. Furthermore, numerical simulations for these tests have been compared with the experimental results and the time history output of the CVS.

The numerical simulation with the presented input parameters was able to capture the contact explosion event with minimal error. These model parameters can further be utilized for future research in contact explosion response of reinforced concrete members. Use of additional increase in the material strength to account for strain-rate effects has been found to be inappropriate. This is due to the fact that a numerical solution using finite element method accounts for the inertial effects of concrete which is responsible for the strain-rate dependency of concrete material.

Consistent results have been observed with rate-effects option deactivated in *MAT_CSCM (Mat_159) constitutive model in LS-DYNA. The shock wave velocity observed from the data recorded by CVS was found to be close to the empirical value reported in the literature. The sensors placed in the crater or the scab zone were damaged and no readings were observed before the damage. Hence, it is proposed to embed the CVS below the neutral axis of the test specimen. This is expected to provide strain developed due to compressive shock wave while it travels away from the point of detonation, as well as the strain due to tensile shock wave after it gets reflected from the back face. Use of CVS in experiments involving contact or near-field explosions has potential, however further improvement is required in calibration and placement of these sensors.

References

Bhalla, S., Shanker, R., Gupta, A., & Kumar, M. P. 2011. Dual Use of PZT Patches as Sensors in Global Dynamic and Electromagnetic Impedance Techniques for Structural Health Monitoring. *Journal of Intelligent Material Systems and Structures,* **22**(16): 1841-1856.

Bhalla, S., & Kaur, N. 2014. Feasibility of Energy Harvesting from Thin Piezo Patches Via Axial Strain (d_{31}) actuation mode. *Journal of Civil Structural Health Monitoring,* **4**(1): 1-15.

Dua, A., & Braimah, A. 2016. *State-of-the-Art in Near-Field and Contact Explosion Effects on Reinforced Concrete Columns*. 5th International Structural Specialty Conference: Canadian Society for Civil Engineering London, Canada, pp. 1:12 (STR-836).

Ducibella, R., & Cunningham, J. 2010. Design Considerations. In D. O. Dusenberry (Ed.), *Handbook for Blast-Resistant Design of Structures*. New Jersey, USA: John Wiley & Sons.

FEMA 426. 2005. *Reference Manual to Mitigate Potential Terrorist Attacks Against Buildings*. Federal Emergency Management Agency (FEMA) USA.

Goel, M. D., Matsagar, V. A., & Gupta, A. K. 2015. Blast Resistance of Stiffened Sandwich Panels with Aluminum Cynosphere Cyntactic Foam. *International Journal of Impact Engineering,* **77**: 134-146.

Hyde, D. 1988. *User's guide for microcomputer programs CONWEP and FUNPRO - Applications of TM 5-855-1*. Vicksburg, MS.

Puryear, J. M. H. 2012. *ALE Modeling of Explosive Detonation on or Near Reinforced-Concrete Columns*. 12th International LS-DYNA Users Conference: LSTC Detroit, USA,

Rigby, S. E., Tyas, A., Clarke, S. D., Fay, S. D., Warren, J. A., Elgy, I., & Gant, M. 2014. *Testing apparatus for the spatial and temporal pressure measurements from near-field free air explosions*. 6th International conference on Protection of structures against hazards: Tianjin, China,

Schwer, L. 2009. Strain Rate Induced Strength Enhancement in Concrete: Much Ado About Nothing. *Proceedings of 7th European LS-DYNA Conference*: DYNAmore Salzburg, Austria

Talakokula, V., & Bhalla, S. 2014. Reinforcement Corrosion Assessment Capability of Surface Bonded and Embedded Piezo Sensors for Reinforced Concrete Structures. *Journal of Intelligent Material Systems and Structures,* **27**(17): 2304-2313.

Trajkovski, J., Kunc, R., Perenda, J., & Prebil, I. 2014. Minimum mesh design criteria for blast wave development and structural response - MMALE method. *Latin American Journal of Solids and Structures,* **11**: 1999-2017.

UFC-3-340-01. 2002. *Design and Analysis of Hardened Structures to Conventional Weapons Effects*. Department of Defense USA.

UFC-3-340-02. 2008. *Design of structures to resist the effects of accidental explosions*. United States Department of Defense Washington, D.C.

UFC-4-010-01. 2007. *DoD Minimum Antiterrorism Standards for Buildings*. Department of Defense (UFC-4-010-01), USA.

UFC-4-010-02. 2007. *DoD Minimum Antiterrorism Standoff Distances for Buildings*. Department of Defense (UFC-4-010-02), USA.

Williams, G. D., & Williamson, E. B. 2011. Response of Reinforced Concrete Bridge Columns Subjected to Blast Loads. *Journal of Structural Engineering,* **137**(9): 903-913.